Dynamic Shear Modulus of Isotropic Elastomers

A. M. Squires, A. R. Tajbakhsh, and E. M. Terentjev*

Cavendish Laboratory, University of Cambridge, Madingley Road, Cambridge CB3 0HE, U.K.

Received July 23, 2003; Revised Manuscript Received December 10, 2003

ABSTRACT: We have investigated the dynamic mechanical behavior of two cross-linked polymer networks with very different topologies: one made of backbones randomly linked along their length; the other with fixed-length strands uniformly cross-linked at their ends. The samples were analyzed using oscillatory shear, at very small strains corresponding to the linear regime. This was carried out at a range of frequencies, and at temperatures ranging from the glass plateau, through the glass transition, and well into the rubbery region. Through the glass transition, the data obeyed the time−temperature superposition principle, and could be analyzed using WLF treatment. At higher temperatures, in the rubbery region, the storage modulus was found to deviate from this, taking a value that is independent of frequency. This value increased linearly with temperature, as expected for the entropic rubber elasticity, but with a substantial negative offset inconsistent with straightforward enthalpic effects. Conversely, the loss modulus continued to follow time−temperature superposition, decreasing with increasing temperature, and showing a power-law dependence on frequency.

1. Introduction

The thermodynamics of rubber elasticity has been the subject of research from the 19th century onward. Theories relating the macroscopic mechanical properties to the entropy of the constituent chain molecules were developed from early in the last century and are well reviewed in ref 1. The classical equilibrium theory of entropic rubber elasticity suggests that the stiffness modulus should simply be proportional to N_x, the density of cross-links (or entanglements, see below), and k_BT, the Boltzmann temperature. Such descriptions were assumed to represent the equilibrium ("long-time" or low-frequency) limit of the mechanical response, assuming that the polymer chains had sufficient time to reach the thermodynamically preferred configuration. (In fact, more recent work[2] has questioned whether such a "long-time" limit exists, or instead some aging processes occur in rubbers at all time scales.)

At lower temperatures or shorter time scales, where the mechanical perturbation and measurement are no longer infinitely slow as compared with the internal rearrangement of polymer chains through different conformations, viscoelastic dynamic behavior is observed. The dynamic behavior of polymers has been understood from theories which were initially developed to describe individual chains in solution[3,4] and then extended to concentrated solutions and polymer melts, including the development of reptation theory.[5,6] Although the detailed dynamic predictions based on the tube model have enjoyed spectacular success over the years, having been tested in a variety of systems, the parallel description of cross-linked networks has been less clear. The entanglement constraints are expected to be much more pronounced in a network, where the disengagement and constraint release by reptation are not available. Although the equilibrium (static) rubber elastic response of polymer networks has been successfully calculated, using several approaches within the tube model,[7,8] the question of whether the equilibrium is ever achieved in mechanical experiment presents an unresolved problem. This requires a consistent theory of dynamic mechanical response over a range of frequencies, from the lower rubber plateau at $\omega \to 0$ to the higher entangled plateau and then to the glassy regime at frequencies above the Rouse level. There is a large body of theoretical literature on this subject, with many advanced insights and predictions. In particular, the calculation of relaxation time spectra (usually denoted $H(\tau)$ in this trade) of phantom chain networks, based on the topological theory of graphs, is well developed.[9−11] As for the real entangled networks, the lower-frequency regimes are described theoretically,[12] but a unified model including the prominent dynamic glass transition has yet to be developed. Also, unless special precautions are taken, it is often hard to ensure that the network cross-linking is homogeneous and not clustered into dense regions and more weakly cross-linked (thus elastically active) regions; see, e.g. ref 13.

Rubber technology heavily depends on an understanding of the response of this complex viscoelastic material to small and large deformations.[14] Despite our everyday experience of highly stretchable elastic bands, an overwhelmingly majority of the practical applications of rubbers explores their response to very small local strains: from automobile tyres and antivibration suspensions to seals and noise insulators. There are two ways in which the mechanical response of rubbers can be probed: by imposing an external strain (a specific component of shear, ϵ) and measuring the stress response, or by applying a force (stress, σ) and detecting the resulting deformation. When the external perturbation is small, one arrives at the linear-response constitutive relationships

$$\sigma(t) = \int_{-\infty}^{\infty} G(t-t')\frac{d}{dt'}\varepsilon(t')\,dt' \;; \quad \sigma(\omega) = \underbrace{\mathcal{FT}\,[G(t)]\;\; i\omega}\;\varepsilon(\omega) \tag{1}$$

where $\mathcal{FT}[...]$ denotes the Fourier transformation. The underlined expression is what one calls the dynamic complex modulus, which, accordingly, is defined as

$$\sigma(\omega) = G^*(\omega)\epsilon(\omega); \quad G^*(\omega) = G' + iG'' \tag{2}$$

Note that, perhaps a little unfortunately, the definition of dynamic shear modulus $G^*(\omega)$ (and similarly the

10.1021/ma035060e CCC: $27.50
Published on Web 01/27/2004

dynamic compliance) is not a direct Fourier transform of the retarded relaxation modulus $G(t - t')$.

By causality, the value of $G(t < t')$ has to be exactly zero to prevent us discovering the future (at $t' > t$) from the current response. A direct consequence of this is the Kramers−Kronig relations between the real and imaginary parts of the complex linear response coefficient. The components of dynamic modulus $G^*(\omega)$ satisfy

$$G'(\omega) = -\mathscr{P}\int_{-\infty}^{\infty} \frac{\omega}{\omega_1} \frac{G''(\omega_1)}{\omega - \omega_1} \frac{d\omega_1}{\pi} \quad \text{and}$$

$$G'(\omega) = \mathscr{P}\int_{-\infty}^{\infty} \frac{\omega}{\omega_1} \frac{G'(\omega_1)}{\omega - \omega_1} \frac{d\omega_1}{\pi} \tag{3}$$

where the integrals are regarded as their principal values. The classical retarded linear constitutive relationships between stress and strain have a simple meaning if one considers two obvious limiting cases. An ideal Newtonian liquid is characterized by the linear relation $\sigma(t) = \eta\dot{\epsilon}(t)$, with η the viscosity, corresponding to $G(t - t') = \eta\delta(t - t')$. In Fourier space, according to the definition above, we have $G^*(\omega) = i\,\omega\,\eta$, a purely imaginary modulus corresponding to $G'' = \omega\,\eta$. The viscous dissipation is directly related to the imaginary part, the "loss modulus" G''. Now consider an ideal elastic solid: clearly $\sigma(t) = G_{eq}\epsilon(t)$, with G_{eq} the shear modulus, corresponding to the constant value $G(t - t') = G_{eq}$. As a result, in the frequency domain, $G' = G_{eq}$—the "storage modulus", defining the amount of elastic energy stored in the material.

In describing the experimental data on polymeric materials, important simplifications may be made by the use of two empirical principles: the Boltzmann superposition principle and the time−temperature equivalence.[15] At very low temperatures (or short times/high frequencies), all polymer materials show glassy behavior. In this regime, the movement of chain segments is too small for the cross-linking to have any effect; the monomers are effectively held in place by the kinetic barriers presented by surrounding "cages". As temperature is increased through the glass transition into the rubbery region, the polymer chains have more freedom from the kinetic constraints and become increasingly constrained by the permanent cross-links. Some features of the dynamic mechanical properties which are specific to cross-linked elastomers in the long-time rubbery regime have been observed and described in terms of a number of models, for example, the "dangling end" hypothesis for long-term stress relaxation.[16]

This paper presents work on two very different "model" elastomers, showing features of the small-strain dynamic mechanical properties over a range of frequencies and temperatures. The motivation for this is 2-fold. First, as more progress is made on general theoretical descriptions which attempt to describe the whole range of behavior, from glassy to rubbery, this work adds to the body of available experimental data which can be used to test trends predicted by different theoretical models. Second, data on pure cross-linked networks serves as a point of reference for more complex elastomers, such as those containing fillers or those with inherent anisotropy caused by attached liquid crystalline groups.

The two elastomers under investigation are a side-chain isotropic elastomer (SCIE) and a uniform isotropic elastomer (UIE). The chemical structures of the two elastomers and the techniques used in their preparation are described in more detail in the next section. The SCIE consists of a polysiloxane backbone, with hydrocarbon side chains, cross-linked with difunctional hydrocarbon cross-linkers. It was originally intended as an isotropic analogue of the nematic elastomer described in ref 17 and is similar to the isotropic side-chain network studied in ref 18. We estimate that approximately 60% of this elastomer (by weight) consists of side chains which do not participate in the cross-linking network but act as a filler, effectively diluting the backbones. Furthermore, although the length of the cross-linker groups is fixed, their positions along the backbone are random, so SCIE is a truly random network with possible free dangling ends and cross-link clusters. In contrast, the UIE network consists of cyclic siloxane junctions, each of which is connected to exactly four difunctional chains acting as network strands of fixed length, similar to the concepts described in ref 19. It contains no side chains and was prepared with a small excess of siloxane junctions, to minimize the numbers of "dangling ends" not participating in the cross-linking network. As a result, the UIE network is much more uniform than that of SCIE. We should, however, point out that there is much room for variation in the ways in which the cross-linking junctions are connected by the strands—for example, one can envisage various different larger cyclic structures consisting of two, three, four, or more connected junctions, so the network topology is not completely uniform as the four-functionality of each junction would imply. Also, we shall see that since all internal space in the UIE material is occupied by network chains, with no filling or effective dilution, the entanglements become important in the elastic response.

In these contrasting materials, we find a comfortingly universal dynamic-mechanical response at low temperatures, during and below the respective glass transitions. The time−temperature ($t-T$) superposition and the WLF analysis work well and allow the construction of master curves. At high temperatures, when the storage modulus of both networks is expected to saturate on the flat rubber plateau, we find a different behavior. The universal (frequency independent) rise in the modulus with temperature makes it impossible to continue the $t-T$ superposition, and the slope of this rise appears to be different from what entropy-based rubber elasticity ideas would suggest. We discuss these findings and their implications at the end of this article.

2. Experimental Section

2.1. Sample Preparation. The component molecules used in the synthesis of the two elastomers are shown in Figure 1. The difunctional compound 1,4-di(11-undeceneoxy)benzene (11UB) serves as a cross-linker in SCIE and acts as a network strand in UIE. It was prepared by the Williamson etherification[20] of hydroquinone and 11-undecene bromide, followed by distillation under reduced pressure (160 °C/0.8 Torr). The SCIE side-group (3-buteneoxybenzene) was synthesized using the Mitsunobu procedure[21] followed by distillation under reduced pressure (100 °C/0.8 Torr). The cyclic siloxane junction used in the preparation of UIE and the siloxane backbone for SCIE are both commercially available, and were obtained from Aldrich.

The elastomer networks were prepared by hydrosilylation of reacting mixtures in toluene at 80 °C for 1 h in the presence of a commercially available platinic acid (COD) catalyst, from

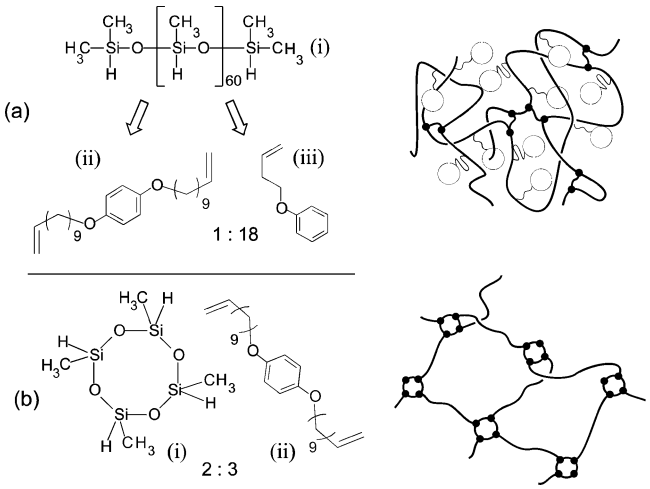

Figure 1. Chemical structures of the materials used described in this work, and their resulting network topology. (a) Components of SCIE: siloxane backbone (i), 11UB cross-linker (ii), and 3-buteneoxybenzene side-group (iii). The molar proportion of 11UB to the side group is 1:18 (10% cross-linking density). (b) Components of UIE: cyclic siloxane cross-linking junction (i) and 11UB strand (iii). This network is linked with a slight excess of cyclic junctions (molar proportion 1:1.5 instead of 1:2 suggested by ideal four-functional junctions) to ensure all strands are linked and not freely dangling.

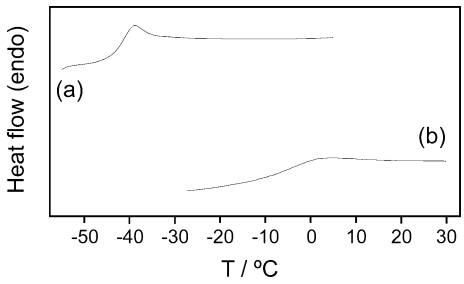

Figure 2. DSC scans on heating of SCIE, curve a, and UIE, curve b. Both scans show the second cycle (which was identical to subsequent cycles), obtained at a rate of 10 °C/min. The two apparent glass transitions were the only thermal feature for each material.

Wacker Chemie. These conditions used were found to be sufficient to allow the reaction, linking the Si−H bond of the siloxane[22] with the terminal vinyl group of 11UB or 3-buteneoxybenzene, to proceed to completion. The toluene solvent was then removed by annealing the samples overnight at 100 °C.

2.2. Thermal Analysis of Phases. Differential scanning calorimetry (DSC) was performed on the two materials, to identify their glass transition temperatures. The two characteristic DSC traces are shown in Figure 2. Both samples have a single glass transition with no other features over the temperature range examined. The values for the glass transition temperature T_g were estimated to be −41 and −6 °C for the SCIE and UIE samples, respectively. Figure 2 also shows qualitatively that the glass transition occurs over a much broader temperature range in the UIE material.

2.3. Dynamic Mechanical Testing. Dynamic mechanical measurements were performed on a VA4000 Viscoanalyzer, from Metravib Rds. A shear strain with an amplitude of $\epsilon_o = 0.002$ was employed. Measurements at different amplitudes confirmed that this was well within the linear response region. Each sample was analyzed over a range of temperatures from the glassy to the rubbery regions, and at each temperature, a range of frequencies between 1 and 200 Hz were employed. Further measurements at low frequencies down to 0.02 Hz were also performed in order to access data for the rubbery region, which could not be inferred assuming time−temperature superposition (see later discussions).

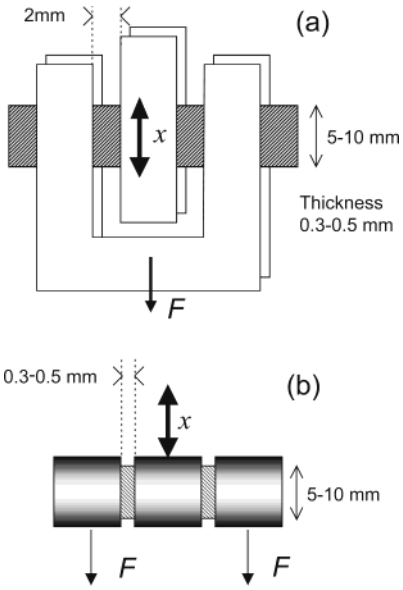

Figure 3. (a) Tape mode, and (b) sandwich mode geometries for DMTA measurements. Samples are illustrated cross-hatched, for clarity, and typical sample dimensions are included. In each case a sinusoidal oscillation is imposed upon the middle section, and its dynamic displacement x is recorded. The dynamic force F exerted on the end sections due to sample shearing is also recorded, and the two parameters used to determine the complex shear modulus G^*.

Two different experimental geometries were employed. These are referred to as "tape" and "sandwich" modes, and the main features and typical sample dimensions are shown in Figure 3. The choice of geometry depended on the stiffness of a sample over the temperature range employed in a given experiment. The tape geometry was used for stiffer samples, toward the glassy region, and was found to give reliable results for shear moduli down to around 10^6 Pa, below which the forces generated were too low to be measured with any degree of confidence. Conversely the sandwich geometry was employed for less stiff samples, toward the rubbery region, and it gives reliable results for shear moduli up to around 10^7 Pa. Above this value, the frictional force between the metal and the rigid sample was insufficient to prevent slippage due to the high forces applied.

Using these two geometries, it was possible to obtain data over several decades of stiffness, from glassy to rubbery behavior. The two sets of results for the same elastomer obtained using different sample geometries were then combined by multiplying all of the storage and loss moduli data from one sample geometry by a single constant value, found by comparing the data over the intermediate stiffness region between 10^6 and 10^7 Pa where measurements could reliably be taken using both geometries. (This corresponds simply to a vertical shift on the graphs we present in this paper, where the moduli are plotted on a log scale.) This scaling factor took values between 0.6 and 1.1, and was assumed to reflect any possible error in measurement of sample dimensions due, for example, to clamping effects. The same constant could be used to match up the data over all frequencies, for both G' and G'', which gives confidence in the described procedure of matching. We note, however, that this represents a small but uncontrollable scaling error in the final actual size of the G' and G'' values quoted. Nevertheless, the main features of this paper are the trends in G' and G'' and in their ratio, rather than their actual values.

3. Results and Discussion

3.1. Temperature and Frequency Dependence. The variation of storage modulus G' with temperature at several fixed frequencies, for both elastomer samples, is shown in Figure 4. Both materials show the same

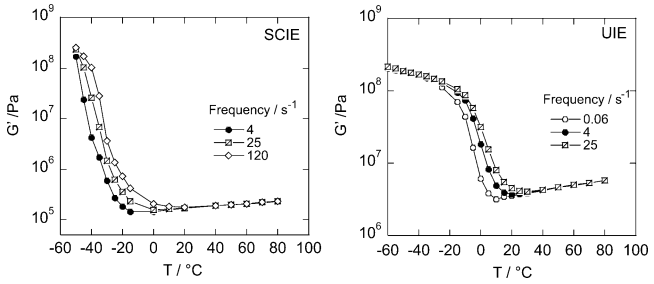

Figure 4. Storage moduli of SCIE and UIE samples as a function of temperature, at several different frequencies. Each curve is constructed by the superposition of data measured using two different sample geometries—see section 2.3 for detail. The high temperature (rubbery) regions of each plot are enhanced and analyzed in greater detail in Figure 9.

general features, as one might expect, which may be divided into three general regions. At low temperatures, both samples are in the glassy region, and they show a storage modulus which is only weakly dependent on both frequency and temperature, taking a value of $G' \approx 10^8-10^9$ Pa. Both samples then show frequency-dependent behavior through the glass transition, a region which will be discussed in more detail throughout this paper. In this region, the magnitude of G' decreases from glassy to rubbery values with increasing temperature, the point of this dynamic glass transition consistently shifting to higher temperatures as the frequency is increased. Finally, at high temperatures, in the "rubbery" region, the behavior becomes independent of frequency, but increases with increasing temperature. The possible reasons for this and its experimental significance will be discussed in more detail in the final section of this paper.

Essentially the same data is shown in Figure 5, which shows the variation in G' with frequency for both samples at different temperatures. The main features shown in these graphs are the frequency-dependent increase in the modulus through the glass transition, and the rubbery response, which is independent of frequency but now increases with increasing temperature. The data through the glass transition may be combined to form a master curve as a single data set, as a function of frequency, by using the empirical time−temperature ($t-T$) superposition principle.[15,23] This effectively allows data sets taken at different temperatures to be superposed by multiplying the actual frequency by a temperature-dependent shift factor, $a(T)$. In a plot where frequency is plotted on a logarithmic scale, as in Figure 5, this simply corresponds to shifting each data set to the left or right by an amount determined empirically, until the curves lie on a single master curve. This method was used to produce the results presented and discussed in the next section. However, an inspection of Figure 5 shows that this approach can only be applied through the glass transition and will not be successful in the rubber plateau region.

3.2. Construction of Master Curves. For each sample, a set of shift factors $a(T)$ were determined empirically to achieve the best superposition of individual data sets for $G'(\omega)$, the loss modulus $G''(\omega)$ and their ratio—the loss factor $\tan \delta = G''/G'$, by only horizontal shifting along the frequency axis. These master curves, for each sample, are shown in Figure 6. The reference temperature, at which the shift factor is $a(T_{ref}) = 1$, was chosen to be $\approx T_g$, the glass transition for each sample (the actual values used were $T_{ref} = -40$ and -5 °C for the SCIE and UIE samples, respectively). The choice of reference temperature for the $t-T$ superposition is rather arbitrary and many advantages could be found in making it a room temperature, thus effectively predicting the values of corresponding moduli at different frequencies as if they were actually mea-

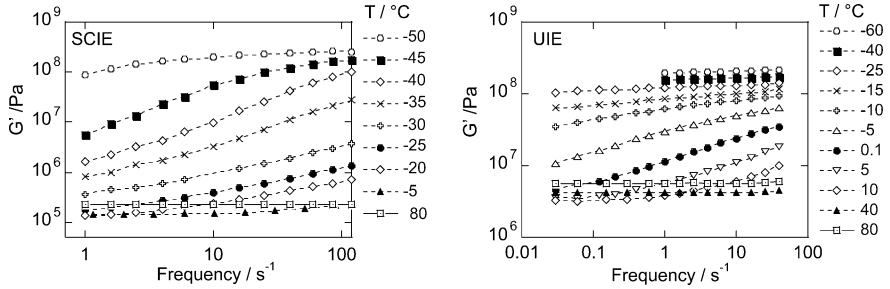

Figure 5. Storage moduli of SCIE and UIE materials as a functions of frequency, at different temperatures.

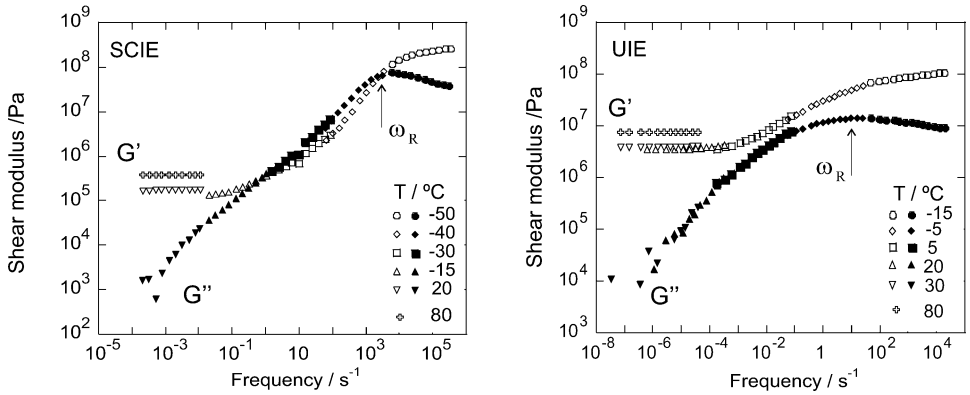

Figure 6. Master curves for $G'(\omega)$ and $G''(\omega)$, for the random SCIE network (for $T_{ref} = -39.9$ °C) and the UIE material (for $T_{ref} = -4.9$ °C). The arrows point to the frequency ω_R corresponding to the Rouse time of network strands. Note the significant increase in G' at high temperatures.

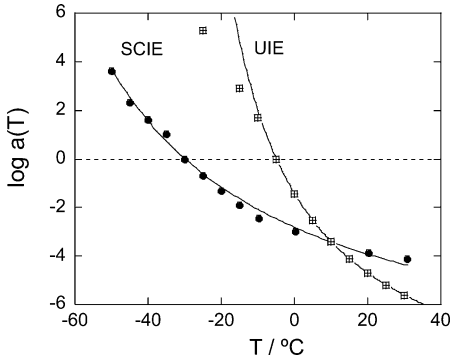

Figure 7. WLF plots showing shift factors $a(T)$, on logarithmic scale, with fits of WLF eq 4, solid lines.

sured without any temperature change. However, here we follow the original proposition of Williams, Landel, and Ferry (WLF)[15] to choose the glass transition as the only characteristic temperature for the amorphous polymer material.

At high temperatures, where the storage modulus shows an increase with temperature that is independent of frequency, the $t-T$ superposition principle cannot succeed. It is clearly not possible to superpose parallel horizontal data sets simply by shifting them to the left or right along the log-frequency axis. In fact, the underlying spirit behind the master curve $G'(\omega)$ is a *prediction* of the response at all different frequencies, as if it were measured at a constant temperature $T = T_{ref}$ (which, of course, is technically impossible over such a great range of frequencies). Such a measurement would have given a continuously lowering G' at lower frequencies, with a debatable question of whether the final equilibrium rubber plateau is ever achievable. In contrast, the G' curves in Figure 6 show a distinct upward step in the modulus at higher temperature, which through $t-T$ superposition would correspond to the low-frequency regime. Despite this problem with G' data at high temperatures, the $t-T$ superposition principle may still be successfully applied to the loss modulus G'', which continues its power-law decay well into the rubbery region.

The shift factors $a(T)$ are represented in Figure 7. The $t-T$ superposition of both samples can be described for the most part by a single curve, given by the empirical WLF relationship[15]

$$\log a(T) = \frac{-C_1(T - T_{ref})}{C_2 + T - T_{ref}} \qquad (4)$$

Some deviations from WLF behavior may be seen at low temperatures, but we could consider them as minor. The values for parameters C_1 and C_2 were fitted to 9.8 ± 0.7 and 47 ± 6, respectively, for the SCIE material, and 10.82 ± 0.05 and 32.5 ± 0.3 for the UIE rubber, ignoring the first two data points. Typical values for these parameters are quoted as $C_1 = 14-18$ and $C_2 = 30-70$ K.[23] Our values for C_1 are therefore a little lower than one might expect, but certainly in the general agreement with the classics of $t-T$ superposition. It is important to emphasize that the same factors were used to successfully superpose the separate data sets for G', G'' and their ratio, the loss factor $\tan \delta$.

3.3. Features of Master Curves. The G' curves in Figure 6 both have a sigmoidal form, representing the transition from glassy to rubbery behavior, as we would expect. In the case of the UIE sample, we could identify a region during this transition, which is locally a straight line on the graph, at the turning point. This corresponds to a "pseudo-power law" behavior, and we can determine a pseudo-power exponent from the slope of the graph at this point, with a value of approximately 0.3. The G' master curve for the SCIE shows at least two different power law regimes through the glass transition. The steepest slope occurs at a scaled frequency of around 1000 Hz, and corresponds to a pseudo-power law exponent of around 1. At lower frequencies, below 100 Hz, the graph approximates to power-law behavior with a lower exponent of around 0.5. The steeper slope of G' variation with frequency seen in the SCIE material may well reflect the same underlying phenomenon as we have seen in the thermal signature of the glass transition, in Figure 2. In contrast, the UIE rubber had a much broader, diffused thermal glass transition, which is also a feature of the α-relaxation in the UIE master curve.

Figure 8 gives a more detailed analysis of power laws involved. The loss modulus G'' is chosen for it, since it has more readily identifiably glass transition frequency, represented as a peak of so-called α-relaxation, and also continues to decrease at low frequencies, unaffected by the unclear (see the discussion below) issues of rubber-

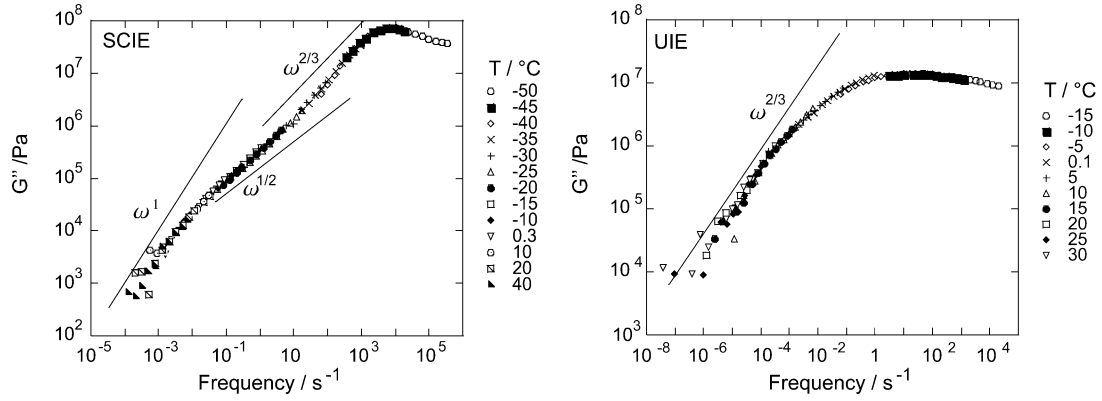

Figure 8. Slopes of characteristic power laws for loss moduli $G''(\omega)$, for SCIE and UIE networks. Despite a much greater regularity of strands in the UIE rubber, its response shows a very diffuse glass transition and a nondistinct power law $\propto \omega^{2/3}$ down to the lowest frequency. In contrast, the SCIE network has a very clear glass transition, the identifiable Rouse regime and turns to the classical viscous response $G'' \propto \omega$ at $\omega \rightarrow 0$.

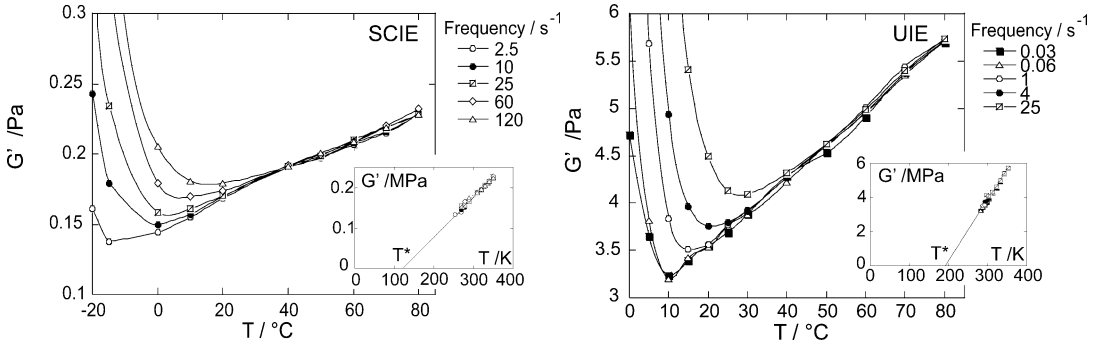

Figure 9. High-temperature region of $G'(T)$ showing the temperature-dependent increase for SCIE and UIE rubbers at a range of frequencies. The insets show the linear regions of $G'(T)$ against the absolute temperature, extrapolated to zero at $T = T^*$; see text. (Note: G' is now plotted on a linear scale.)

elastic modulus $G'(T)$. At frequencies just below the glass transition, the loss modulus drops with a scaling, which can be identified as $G'' \propto \omega^{2/3}$. One could make a connection with the Zimm model, proposing an exponent of 0.66, although the conceptual relation between the dilute polymer solution with hydrodynamic interactions[4] and our 10%-cross-linked dry rubber is quite unconvincing. (We note that in a recent study of liquid crystalline rubbers, an isotropic side-chain material similar to our SCIE has been studied—and the Zimm-like exponent of 0.66 was also reported.[18]) Even if one attempts to make such a connection by identifying the bulky side groups of SCIE, attached to the network by flexible spacers, with a solvent diluting a backbone, it certainly does not hold for the UIE rubber.

Further away from the glass transition, the two materials show very different behavior. For SCIE, there is an indication of a shoulder appearing at scaled frequencies of around 1 Hz (corresponding to temperatures of around −20 °C). One could argue that we see the (much anticipated) Rouse scaling $G'' \propto \omega^{1/2}$, which then turns into a more steep decay at the lowest frequencies, very much resembling the classical viscous dissipation, $G'' \propto \omega$. It would have been very nice indeed to find a rubber material with a low-frequency elasticity following the simple Debye relaxation ($G' \sim G_{eq} + \eta(\omega\tau)^2$; $G'' \sim \eta\,\omega\tau$). Usually, cross-linked rubbers have a more complex response. In contrast to SCIE, the uniform network of UIE does not seem to fall into any such behavior even at the lowest frequencies, when the storage modulus has well and truly lost its frequency dependence.

We note in passing the different levels of the loss factor tanδ for the two elastomers. Although we do not plot these explicitly, one can see from the data in Figure 6 that in the UIE network the ratio of G'' to G' is always less than one; in fact, the maximum tan $\delta \approx 0.55$ is reached in a narrow frequency range. In contrast, the SCIE data shows the broad region of scaled frequency, between 1 and 3000 Hz, where G'' is greater than G'. The loss factor reaches the maximum of tan $\delta \approx 2.4$ and is in excess of 2 between 30 and 600 Hz. This is surprisingly high, and may suggest that the presence of side chains, capable of motion independent of the backbones, contribute to the high damping behavior observed in side-chain nematic elastomers.[17,24]

3.4. Rubber Plateau. In the high-temperature/low-frequency limit, both samples show what appears to be the equilibrium rubbery response, where G' becomes completely independent of frequency, but increases with increasing temperature. As we have seen above, this means that $t-T$ superposition cannot be applied to the storage modulus in this region, although it still applies to the data for tan δ and G''.

Let us examine the data for $G'(T)$ in this region in more detail; see Figure 9. Both materials show a linear increase in G' with temperature. This was found to be reversible and reproducible, thus ruling out the possibility of the behavior being caused by some chemical reaction or degradation. The data for the linear increase in G' with temperature in Figure 9 is described by the fitting

$$G' = N_0(T - T^*), \quad \text{with} \begin{cases} \text{SCIE:} & N_0 \approx 10^3\ (\text{Pa/K}), & T^* \approx 121\ \text{K} \\ \text{UIE:} & N_0 \approx 3.6 \times 10^4\ (\text{Pa/K}), & T^* \approx 192\ \text{K} \end{cases} \tag{5}$$

In general, a linear increase in shear modulus with temperature is to be expected from the entropic origin of rubber elasticity. The frequency-independent storage modulus G' is in this region approximately equal to the equilibrium rubber shear modulus μ. The basic model of entropic elasticity of a phantom chain network[1] yields $\mu = c_p k_B T$, where c_p is the number of network strands per unit volume (directly related to the cross-linking density N_x). Modern advanced theories, involving the junction point fluctuations, excluded volume effects and dense entanglements in a rubbery network,[25,26] provide exactly the same expression in the linear-response limit (at small deformations), but with the constant c_p dominated by the number of entanglements per network strand, Z. Crudely, since different models offer slightly different values of the numerical factor of order of unity, one has $\mu \approx N_x Z k_B T$.

We have three ways of estimating the effective strand density c_p. First of all we can obtain a nominal estimate by inspecting the chemical composition of the network. In this approach, we must first define the chemical species corresponding to one elastically active "strand". We then calculate its mass from the molar weights of its components. From this we obtain its volume, assuming its density to be the same as the overall density of the material, which we can determine experimentally. (This assumption requires that we chose a strand whose composition—the ratios of main chains, side chains and cross-linkers—is the same as that of the sample as a whole.) In the SCIE, such a strand is made up of half of a 11UB cross-linker, nine mesogenic side groups and ten Me-SiH−O units from the siloxane backbone (Figure 1, parts a(ii), a(iii), and a(i) respectively). In the UIE,

Table 1. Estimates of an Effective Density of Network Strands (the Entropic Coefficient), c_p, Obtained in Three Different Ways Described in the Text (Labeled as the Argument in Each Column)

sample	$c_p(\rho)$, m^{-3}	$c_p(G')$, m^{-3}	$c_p(dG/dT)$, m^{-3}
SCIE	3×10^{26}	4.1×10^{25}	7.2×10^{25}
UIE	1.1×10^{27}	8.5×10^{26}	2.6×10^{27}

we have considered a single strand to consist of one 11UB molecule (Figure 1, part b(ii)) and two-thirds of a cyclic siloxane cross-linking junction (Figure 1, part b(i)). Using measured values for the densities of SCIE and UIE of 1.08 ± 0.02 and 1.04 ± 0.01 g cm^{-3}, we estimate the volumes of the respective elastically active strands as 3.3×10^{-27} and 9.2×10^{-28} m^3. The inverse of these volumes give the values for strand density listed as $c_p(\rho)$ in the first column of Table 1.

Second, one could estimate c_p from the absolute values of frequency-independent elastic modulus on the "rubber plateau", Figure 9. The second column of Table 1 gives these values. Finally, we can find the effective strand density by literally taking the slope $dG'/d(k_BT)$ from the data in Figure 9 and thus obtain a third value for c_p, for each material. Since the linear extrapolations cross the T-axis at positive T, this estimate gives higher values than those from the modulus magnitude for both our networks. Both of the last two methods are simply different ways of inferring the strand density from the mechanical properties, and so would include both the chemical cross-links and physical entanglements in the networks.

The important feature that we notice from the comparison of values in the table is that for SCIE the rubber-elastic modulus is much lower than the chemical composition would suggest, by nearly an order of magnitude. The effective strand density inferred from the chemical composition is much larger than the values estimated from the modulus. The only reasonable explanation for this is cross-link clustering. Indeed, in such a network one could easily envisage that aliphatic 11UB molecules were partially phase separated from siloxane chains before the cross-linking reaction. In contrast, in UIE the distribution of cyclic cross-linking groups is necessarily homogeneous and, not surprisingly, we see a better correlation between values suggested from the modulus and that estimated from the chemical composition. This also implies that, in UIE, there is no significant entanglement of network strands. This, again, is expected because the network was prepared in a swollen state, with chains stretched and not capable of topological entanglement—and then deswollen into its final state. One cannot make such an assumption about the randomly linked SCIE; this makes it impossible to separate the effect of cross-link clustering (leading to the decrease in modulus) and entanglements (increasing the rubber modulus). Most likely, both effects are in action.

In the discussion of entropic rubber elasticity, we must not forget the result evident from Figure 9, that the extrapolated $G'(T)$ lines do not cross zero at $T = 0$ K. The fitting results of the eq 5 indicate that this would occur at −81 °C (192 K) for UIE and at −152 °C (121 K) for the SCIE rubber. The values are significantly above absolute zero. Accordingly, the values in the third column Table 1, measuring the slope $dG/d(k_BT)$ on the "rubber plateau", are significantly higher than the parallel value measuring the modulus itself, by a factor of 1.8 in SCIE and a factor of 3 in UIE. This linear but nonproportional relation between the modulus and the temperature is surprising, and one for which we do not immediately propose an explanation. A component of stress due to potential energy[27] would be expected to show a positive value for the modulus, when extrapolated to absolute zero. Note that in our experiments the sample is held in a sandwich shear geometry, where it is constrained to a fixed thickness in the z-direction, and so thermal expansion in this direction cannot occur; any thermal expansion or contraction occurring in the $x-y$ plane is effectively prohibited as well, since in the sandwich measuring geometry this plane is constrained between the plates. This represents a difference from measurements of the rubber modulus done in extension of laterally unconstrained samples.

4. Conclusions

Our side-chain SCIE material is very similar to a nonmesomorphic network synthesized and analyzed by Stein et al.[18] Both our elastomers and theirs show features, which Stein et al. have modeled using a modified Zimm model, in which the diluted state of backbone chains is achieved by the large amount of volume-filling side groups. The model features include a power-law exponent of about $^2/_3$ and a value of G' that is lower than G'', giving rise to tan δ values greater than 1. The deviation in the storage modulus G' behavior from that predicted by the standard Zimm model could be explained by the influence of the high- and low-frequency plateaus. However, it is conceptually hard to link such a model with the results on our UIE rubber, which is chemically very different from side-chain polymer networks and has been deliberately designed to minimize all network effects apart from the flexible network strands themselves. Nevertheless, the master curves for both G' and $G''(\omega)$ appear to show the same Zimm-like behavior. This leads us to believe that the power-law exponent of $^2/_3$, seen in our experiments, and in others, is only coincidentally related to that of the classical Zimm model. Indeed, a number of topological theories[10,11] predict power laws stemming from the complex distribution of relaxation times depending on the (phantom) network topology.

This discussion highlights the unfortunate state of current theoretical understanding of dynamic mechanical response of polymer networks. Empirical models could be devised in large numbers, suggesting various relaxation time spectra and enthalpic corrections and successfully interpolating some groups of experimental results—but such models always describe only a part of the full set of properties of a material and offer no real physical insight into them. It appears that the success story of the molecular understanding of polymer dynamics is not readily transferred into the cross-linked networks of the same chains. On one hand, progress is clearly possible through the incorporation of ideas of Rouse−Zimm dynamics into the tube model of end-constrained chains. On the other hand the findings highlighted in Figure 9, that the low-frequency modulus behaves as $G' = -\text{const} + c_p k_B T$ (with a substantially negative constant) and that the value of the modulus does not correspond to the slope $dG'/d(k_BT)$, indicate that purely entropic theories will never be completely successful. The challenge in developing a consistent dynamical theory of rubbery networks remains widely open after more than 50 years since the first theoretical

efforts by Flory[28,29] and classical experiments by Ferry et al.[30] and others.

References and Notes

(1) Treloar, L. R. G. *The Physics of Rubber Elasticity*, 3rd ed.; Clarendon Press: Oxford, England, 1975.
(2) Clarke, S. M.; Elias, F.; Terentjev, E. M. *Eur. Phys. J. E* **2000**, *2*, 335.
(3) Rouse, P. E. *J. Chem. Phys.* **1953**, *21*, 1272.
(4) Zimm, B. H. *J. Chem. Phys.* **1956**, *24*, 269.
(5) de Gennes, P.-G. *J. Chem. Phys.* **1971**, *55*, 572.
(6) Edwards, S. F. *J. Chem. Phys.* **1971**, *55*, 572.
(7) Edwards, S. F.; Vilgis, T. A. *Rep. Prog. Phys.* **1988**, *51*, 243.
(8) Mergell, B.; Everaers, R. *Macromolecules* **2001**, *34*, 5675.
(9) Graessley, W. W. *Macromolecules* **1980**, *13*, 372.
(10) Kloczkowski, A.; Mark, J. E.; Frisch, H. L. *Macromolecules* **1990**, *23*, 3481.
(11) Blumen, A.; Jurjiu, A.; Koslowski, T. *Macromol. Symp.* **2003**, *191*, 141.
(12) Edwards, S. F.; Takano, H.; Terentjev, E. M. *J. Chem. Phys.* **2000**, *113*, 5531.
(13) Schimmel, K. H.; Heinrich, G. *Colloid Polym. Sci.* **1991**, *269*, 1003.
(14) Roberts, A. D. *Natural Rubber Science and Technology*; Clarendon Press: Oxford, England, 1988.
(15) Ferry, J. D. *Viscoelastic Properties of Polymers*, 2nd ed.; Wiley: New York, 1970.
(16) Curro, J. G.; Pincus, P. *Macromolecules* **1983**, *16*, 559.
(17) Clarke, S. M.; Hotta, A.; Tajbakhsh, A. R.; Terentjev, E. M. *Phys. Rev. E.* **2002**, *65*, 021804.
(18) Stein, P.; Assfalg, N.; Finkelmann, H.; Martinoty, P. *Eur. Phys. J. E* **2001**, *4*, 255.
(19) Mark, J. E. *Adv. Polym. Sci.* **1982**, *44*, 1.
(20) Brown, W. H.; Foote, C. F. *Organic Chemistry*, 2nd ed.; Sounders College Publishing: 1998.
(21) Mitsunobu, O. *Synthesis* **1981**, *1*, 1.
(22) Apfel, M. A.; Finkelmann, H.; Janini, G. M.; Laub, R. J.; Luhmann, B. H.; Price, A.; Roberts, W. L.; Shaw, T. J.; Smith, C. A. *Anal. Chem.* **1985**, *57*, 651.
(23) Strobl, G. R. *The Physics of Polymers*, 2nd ed.; Springer, New York, 1997.
(24) Clarke, S. M.; Tajbakhsh, A. R.; Terentjev, E. M.; Remillat, R.; Tomlinson, G. R.; House, J. R. *J. Appl. Phys.* **2001**, *89*, 6530.
(25) Ball, R. C.; Doi, M.; Edwards, S. F.; Warner, M. *Polymer* **1981**, *22*, 1010.
(26) Higgs, P. G.; Ball, R. C. *Europhys. Lett.* **1989**, *8*, 357.
(27) Shen, M. C.; McQuarrie, D. A.; Jackson, J. L. *J. Appl. Phys.* **1967**, *38*, 791.
(28) Flory, P. J. *Principles of Polymer Chemistry*; Cornell University Press: Ithaca, NY, 1953.
(29) Erman, B.; Mark, J. E. *Structure and Properties of Rubberlike Networks*; Clarendon Press: Oxford, England, 1997.
(30) Ferry, J. D.; Grandine, L. D.; Fitzgerald, E. R. *J. Appl. Phys.* **1953**, *24*, 911.

MA035060E